ACS OMEGA

http://pubs.acs.org/journal/acsodf

Article

Non-Conventional Fluorescence and Cytotoxicity of Two Aliphatic Hyperbranched Polymer Dots Having Poly(amic acid) Structures: Implications for Labeling Nanodrug Carriers

Yu-Yu Chen, Siao-Cian Fan, Chang-Cheng Chang, Jian-Cheng Wang, Hsiu-Mei Chiang, and Tzong-Yuan Juang*

Cite This: *ACS Omega* 2021, 6, 33159−33170

Read Online

ACCESS | Metrics & More | Article Recommendations | Supporting Information

ABSTRACT: In this study, we used one-pot A_2 + B_3 polymerizations to synthesize two aliphatic + alicyclic polymer dots (PDs) having non-conjugated hyperbranched structures, employing two types of dianhydrides as the A_2 components, possessing bridged bicyclic alkene (PD-BT) and non-alkene (PD-ET) units, and Jeffamine T403 polyetheramine (T403) as the B_3 components. We prepared PD-ET from commercially available ethylenediaminetetraacetic dianhydride (EDTAD, A_2) and T403 (B_3) and PD-BT from bicyclo[2.2.2]oct-7-ene-2,3,5,6-tetracarboxylic dianhydride (BCDA, A_2) and T403 (B_3). These two types of PDs possessed non-conjugated hyperbranched poly(amic acid) structures with terminal amino functional groups. PD-BT and PD-ET exhibited non-conventional fluorescence with emissions at 435 and 438 nm, respectively, and quantum yields of 12.8 and 14.0%, respectively. The fluorescence intensity of PD-ET was influenced by the pH, but PD-BT was less affected because of its rigid aliphatic bridged bicyclic structure. In aqueous solutions, the sizes of the PD-BT and PD-ET nanoparticles were 3−5 nm, and their net charges can be adjusted by varying the pH. These PDs were non-cytotoxic toward human MCF-7 breast cancer cells and human keratinocyte HaCaT cells at concentrations of 50 μg mL^{-1} for PD-BT and 500 μg mL^{-1} for PD-ET. Confocal microscopic bioimaging revealed that the PDs were located within the cells after treatment for 6 h. These PDs were easy to prepare, highly water-soluble, and possessed a large number of peripheral functional groups for further modification. Combined with their non-conventional fluorescence, they appear to have potential uses in bioimaging and as drug-labeling carriers.

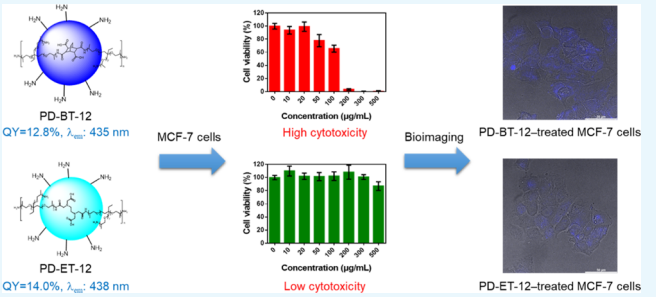

1. INTRODUCTION

Fluorescent carbon nanomaterials (e.g., carbon dots) having high water dispersibility and sizes below 10 nm have been applied biomedically as drug carriers, as diagnostic and therapeutic biomedical tools, and in bioimaging.[1−7] According to their carbon nanostructures, carbon dots can be divided into three groups: graphene quantum dots, carbon nanodots, and polymer dots (PDs).[4,5,8] PDs have been prepared previously from non-conventional fluorescent polymers featuring non-conjugated aliphatic chromophores (containing N, O, S, and P atoms) and triple or double bonds (e.g., C═O and C≡N).[9−14] The mechanisms through which non-conventional fluorescent polymers generate stable fluorescence appear to be cluster-triggered emission (CTE) and aggregation-induced emission (AIE),[15−18] where the lone pairs of electrons and the π-orbitals of the aliphatic moieties produce non-photobleaching fluorescent effects.[12,13] These non-conventional fluorescent polymers can be classified as PDs when their particle sizes are on the nanoscale in aqueous surroundings.[19] In addition, Zhu et al. suggested that PDs could be divided into conjugated and non-conjugated PDs according to the nature of their π-conjugated systems and fluorophores.[12] In a previous study, we prepared non-conjugated fluorescent hyperbranched PDs that were fully water-soluble and exhibited fluorescence quantum yields (QYs) as high as 23% (Em: 395 nm); these entirely aliphatic structures, which had N atoms as their points of branching and an abundance of C═O functional groups, displayed non-conventional fluorescence.[13,20]

Non-conventional fluorescent polymers have been known for several years; they include poly(amido amine) (PAMAM), poly(ethylene diamine) (PEI), and poly[(maleic anhydride)−*alt*−(vinyl acetate)] (PMV).[15] Zhu et al. have synthesized hyperbranched (*hb*) and linear (*l*) aliphatic PAMAMs, both of

Received: October 5, 2021
Accepted: November 10, 2021
Published: November 19, 2021

Scheme 1. (a,b) One-Pot Syntheses of PDs (a) PD-BT-12 and (b) PD-ET-12; (c) Schematic Representation of the A_2 + B_3 Polymerization

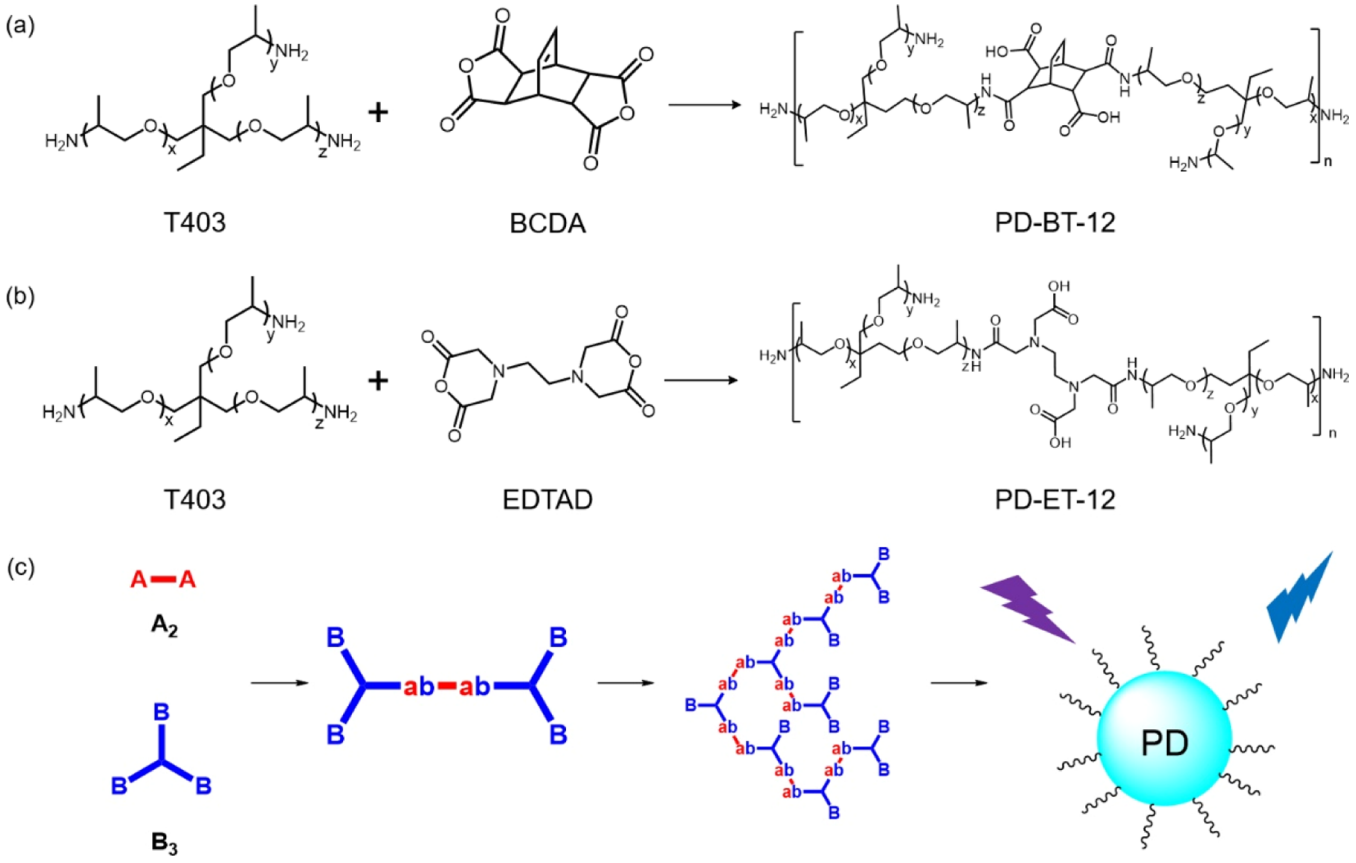

which produced blue fluorescence (450 nm) upon excitation at 380 nm. The fluorescence intensity of *l*-PAMAM was stronger than that of *hp*-PAMAM in dilute solutions, which is the result of different interactions between the amido and amino groups in the intra- and interchain clusters. Nevertheless, both of these PAMAMs displayed fluorescence as a result of AIE.[21] Stiriba et al. prepared fluorescent hyperbranched and linear aliphatic PEIs that did not feature any conventional fluorescent chromophores; methylation and oxidation of the amino groups of the PEIs enhanced the fluorescence intensity.[22] Those two studies revealed that non-conventional fluorescence could arise from polymers possessing amino groups. Tang et al. synthesized a PMV copolymer that produced fluorescence through clustering of C═O groups; furthermore, it exhibited diverse forms of fluorescence when varying the solvent [tetrahydrofuran (THF), *N*-methyl-2-pyrrolidone, and *N*,*N*-dimethylformamide (DMF)].[23]

Typically, fluorescent hyperbranched PDs are highly branched macromolecules having globular structures and conjugated systems.[24] Hyperbranched PDs have been synthesized in three ways: condensation polymerization, addition reactions, and ring-opening polymerization (ROP). Unal et al. employed dropwise addition to control the structural regularity of hyperbranched PDs.[25] In this present study, we synthesized two PDs by combining a dropwise method with condensation polymerization using an A_2 + B_3 strategy, involving the ring opening of a dianhydride (A_2) through a reaction with a triamino compound (B_3). This simple one-pot synthesis allowed control over the nature of the surface functional groups. Interestingly, our resulting PDs were non-conventional fluorescent polymers having hyperbranched structures and nanoscale dimensions in aqueous solutions.

We synthesized two non-conventional fluorescent PDs—PD-BT and PD-ET—from two types of dianhydrides as the A_2 components (possessing bridged bicyclic alkene and non-alkene structures, respectively) and Jeffamine T403 polyetheramine as the B_3 component. The resulting PDs possessed relatively rigid bridged bicyclic and flexible linear structures, respectively, resulting in different fluorescence properties upon adjusting the pH. They also exhibited different cytotoxicities toward human MCF-7 breast cancer cells and human keratinocyte HaCaT cells, with confocal microscopy images revealing that the PDs could be positioned within these cells. These non-conventional fluorescent PDs were easy to prepare, had high water-solubility, and featured a large number of peripheral functional groups that could potentially be modified to develop drug-labeling carriers.

2. RESULTS AND DISCUSSION

2.1. Preparation of PDs. We used an A_2 + B_3 strategy for the one-pot syntheses of PD-BT and PD-ET (Scheme 1a,b). As our two types of A_2 molecules, we selected BCDA and EDTAD, possessing bridged bicyclic alkene or non-alkene structures, respectively. These PDs were obtained through condensation polymerizations, in which the amino groups of the B_3 compound reacted with the two dianhydrides (A_2). For both PD-BT-12 and PD-ET-12, we adopted a molar ratio of A_2 to B_3 of 1 mmol:2 mmol to give a ratio of the anhydride and amino functional groups of 1:3. We added a solution of A_2 dropwise into a solution of B_3 at 0 °C and then slowly warmed

https://doi.org/10.1021/acsomega.1c05537
ACS Omega 2021, 6, 33159−33170

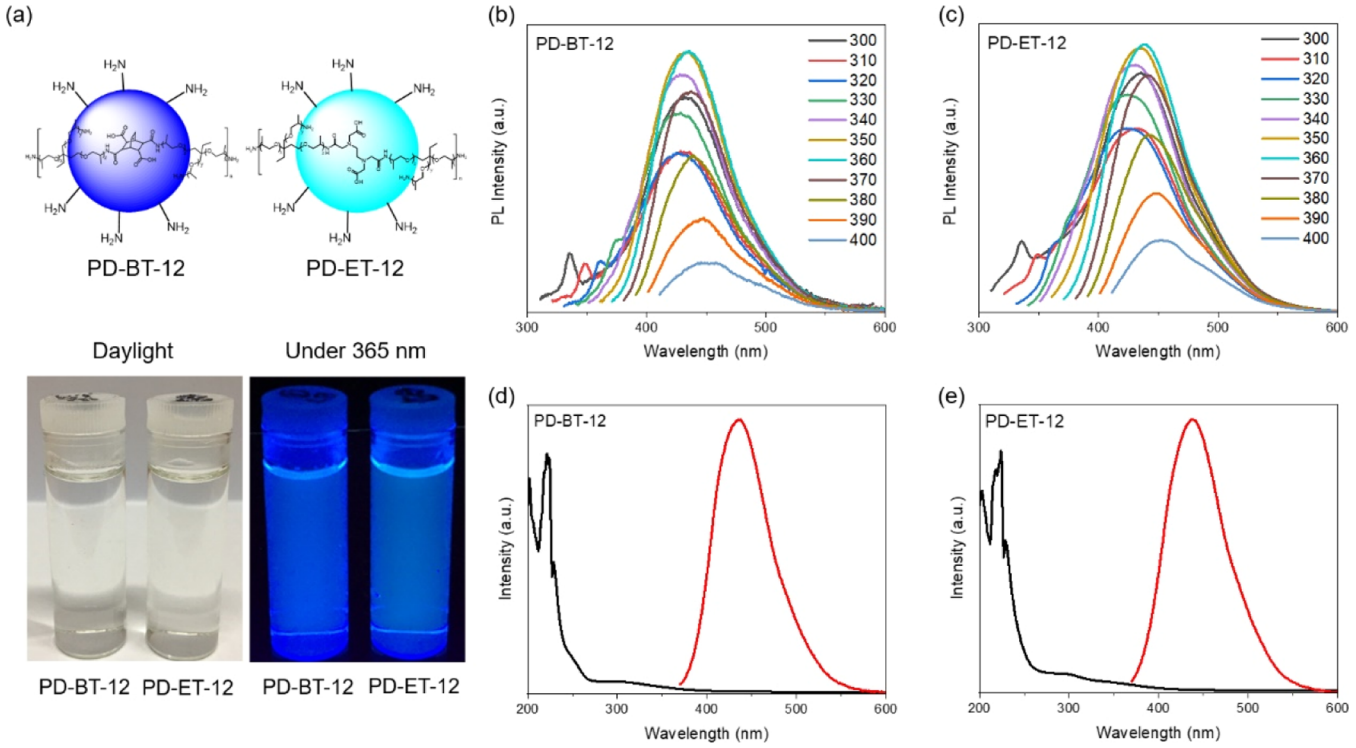

Figure 1. (a) Photographs of PD solutions exposed to daylight and UV light (365 nm). (b,c) PL spectra of (b) PD-BT-12 and (c) PD-ET-12 recorded at various excitation wavelengths. (d,e) PL (red lines) and UV−vis absorption (black lines) spectra of aqueous solutions of (d) PD-BT-12 and (e) PD-ET-12.

the mixture to room temperature, with a total reaction time of 20 h (Scheme 1c). Dialysis of the PD solutions resulted in the removal of any monomers and other small molecules, providing PDs with molecular weights of greater than 3500 g mol^{-1}; we could not determine the molecular weights through gel permeation chromatography (GPC) because our PDs were insoluble in THF and DMF. The polymerization yields of PD-BT-12 and PD-ET-12 were 66.2 and 44.3%, respectively. The resulting PDs dispersed well in water.

2.2. Fluorescence of PDs. We placed solutions of our PDs (1 mg mL^{-1}) under light at 365 nm to observe their fluorescence emissions (Figure 1a). The optimal excitation wavelength of the PDs was 360 nm, and the emission wavelengths of PD-BT-12 and PD-ET-12 were 435 and 438 nm, respectively (Figure 1b,c). The QYs of PD-BT-12 and PD-ET-12 were 12.8 and 14.0%, respectively. The UV−vis absorption spectra of PD-BT-12 (Figure 1d) and PD-ET-12 (Figure 1e) each featured a signal at a wavelength of 202 nm for their amide bonds, a strong absorption peak at 224 nm for the $\pi-\pi^*$ transitions of their C═O bonds, and signals for the $n-\pi^*$ transitions of their C═O and amino groups at 300−400 nm.[26−28]

Solutions of PD-BT-12 and PD-ET-12 in water at a concentration of 1 mg mL^{-1} exhibited essential values of pH of 9.0 and 8.4, respectively. We adjusted the pH of these aqueous PD solutions to 4, 7, and 10, using NaOH and HCl, and observed their fluorescence under daylight and UV light (Figure 2a−d). The intensity of the fluorescence of PD-BT-12 did not change significantly upon increasing the pH, but for PD-ET-12 it decreased accordingly (Figure 2e,f). The QYs of PD-BT-12 at pH 4, 7, and 10 were 13.1, 15.1, and 13.1%, respectively (Figure 2g); for PD-ET-12, they were 17.9, 14.6, and 9.1%, respectively (Figure 2h). Thus, the QYs of PD-BT-12 in neutral, acidic, and basic aqueous solutions were approximately in the range 13−15%. We suspect that this consistent behavior was due to the BCDA monomer (A_2) possessing alkene units and a bridged bicyclic structure, resulting in PD-BT-12 having a relatively rigid structure that was unaffected by its aqueous environment. In contrast, the variable QYs of PD-ET-12 might have been due to its EDTAD monomer (A_2) having a relatively flexible structure. Moreover, PD-BT-12 and PD-ET-12 possessed amino groups at their PD surfaces and carboxyl groups within their PD structures. When we added base (NaOH) to the PD solutions, the carboxylate anions would coordinate Na^+ cations, with the flexible PD structure being better able to accommodate a greater distance between the C═O units. In this case, the decrease in QY was possibly due to a decrease in the CTE effect. Moreover, when PD-ET-12 experienced an acidic environment, its amino groups and tertiary amine became protonated. The positively charged NH_3^+ units and tertiary amino moieties at branching sites would undergo charge repulsion to form a more rigid structure with a shorter distance between the C═O groups. Further increasing the pH to 10 decreased the fluorescence. The decrease of fluorescence intensity is consistent with that of a similar tertiary alkylamino structure NH_2-terminated PAMAM dendrimer,[29] in which the fluorescence increased gradually when the pH decreased from 10 to 4. We also found that our PD-BT-12 and PD-ET-12 showed a strong emission at 435 and 438 nm with the optimal excitation at 360 nm, which was close to fourth generation poly(amido amine) PAMAM for emission at 450 nm with excitation at 390 nm. These results indicated that our two PDs with poly(amic acid) structures and PAMAM with poly(amido amine)[29] and a tertiary amine backbone with a NH_2-terminated group exhibited a similar fluorescent behavior.

https://doi.org/10.1021/acsomega.1c05537
ACS Omega 2021, 6, 33159−33170

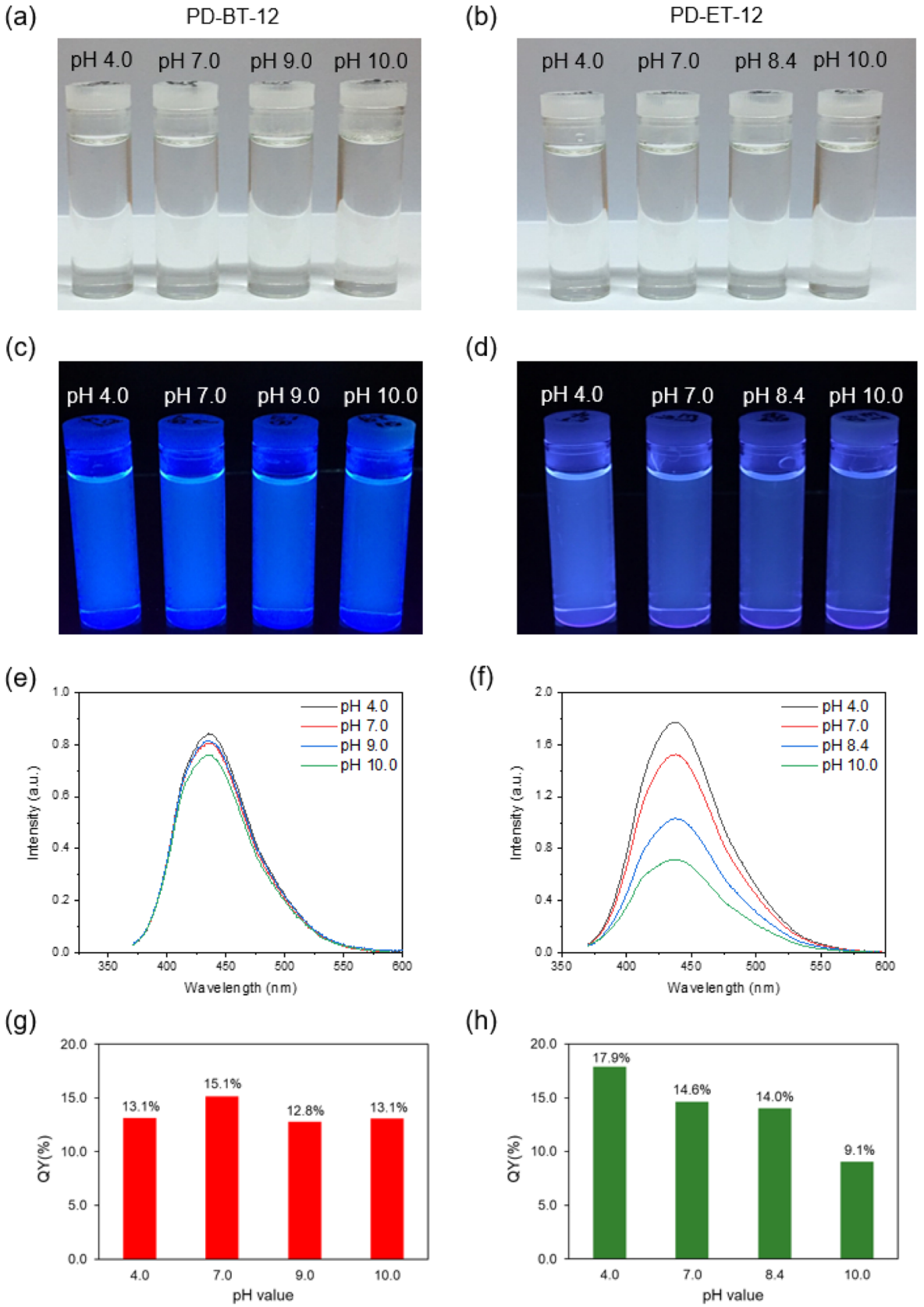

Figure 2. (a–d) Photographs of solutions of (a,c) PD-BT-12 and (b,d) PD-ET-12 at various values of pH under (a,b) daylight and (c,d) UV light. (e,f) PL spectra and (g,h) QYs of solutions of (e,g) PD-BT-12 and (f,h) PD-ET-12 at various values of pH.

Table 1 summarizes the polymerization yields, fluorescence behavior, particle sizes, amine values, and atomic compositions of the PDs. The polymerization yield of PD-BT-12 (66.2%) was higher than that of PD-ET-12 (44.3%), but their QYs and

https://doi.org/10.1021/acsomega.1c05537
ACS Omega 2021, 6, 33159−33170

Table 1. Physical Properties of PDs

name	molar ratio A_2	molar ratio B_3	functional group ratio anhydride/amino	yield (%)	PL[a] Ex (nm)	PL[a] Em (nm)	QY[b] (%)	DLS[c] (nm)	amine value[d] (mequiv g^{-1})	atomic composition[e] (%) C	O	N
BCDA/T403												
PD-BT-12	1	2	1:3	66.2	360	435	12.8	3.0 ± 0.5	3.0	73.0	21.3	5.6
PD-BT-21	2	1	4:3	17.7	cross-linked and non-water dispersible							
EDTAD/T403												
PD-ET-12	1	2	1:3	44.3	360	438	14.0	2.7 ± 0.4	2.3	69.1	20.9	10.0
PD-ET-21	2	1	4:3	21.7	cross-linked and non-water dispersible							

[a]Excitation and relatively high-intensity emission wavelengths of the PD, determined using fluorescence spectroscopy. [b]QY of the PD, calculated from UV−vis absorption and integrated fluorescence spectra, according to the relative fluorescence QY equation. [c]Average particle size of the PD, determined using DLS. [d]Amine titration value. [e]Atomic composition of the PD, determined using X-ray photoelectron spectroscopy (XPS).

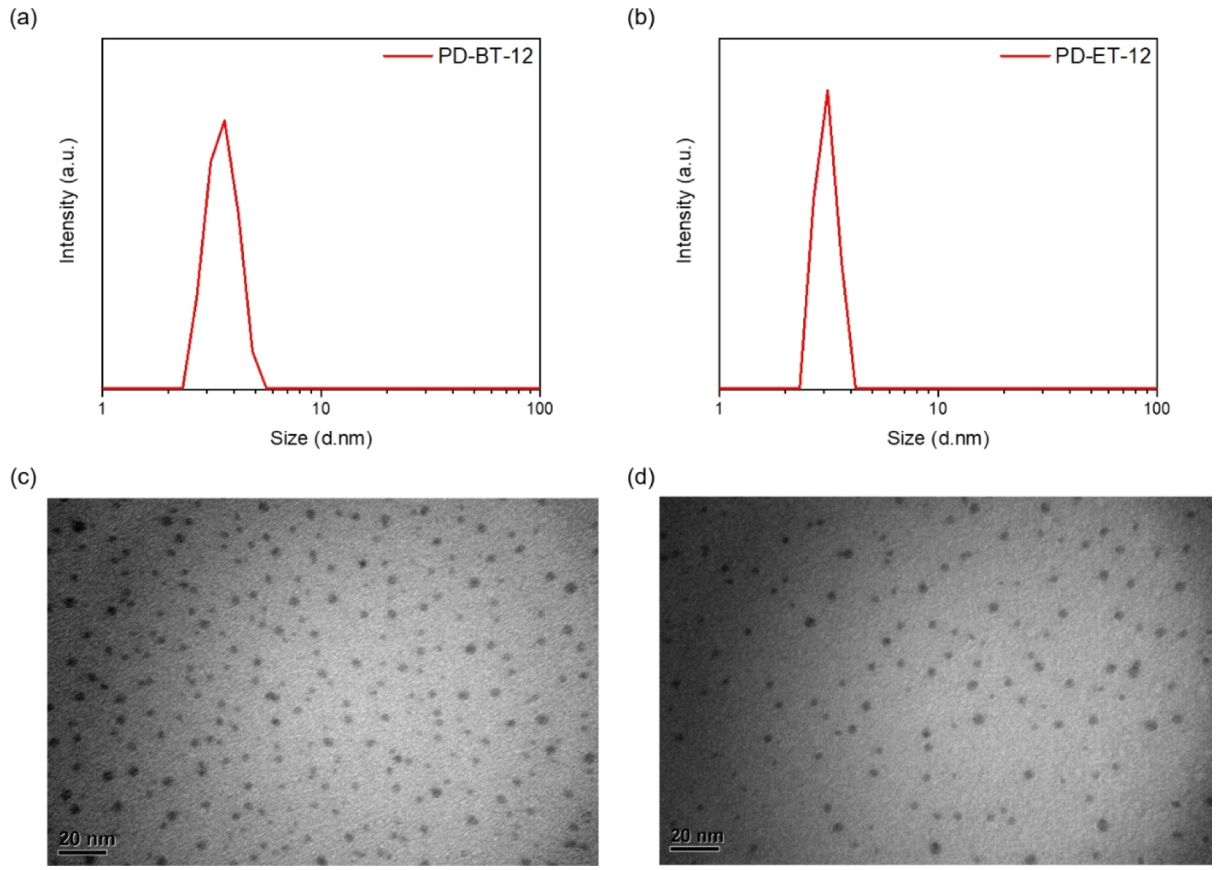

Figure 3. (a,b) DLS histograms and (c,d) HRTEM images of (a,c) PD-BT-12 and (b,d) PD-ET-12.

particle sizes were almost identical at both pH 9.0 and 8.4. The amine values of PD-BT-12 and PD-ET-12, determined through titration, were 3.0 and 2.3 mequiv g^{-1}, respectively. The two PDs both contained C, O, and N atoms; the N-atom content of PD-ET-12 (10.0%) was higher than that of PD-BT-12 (5.6%) because the former was prepared from the N-atom-rich EDTAD monomer. Notably, when we attempted to prepare PD-BT-21 and PD-ET-21 at an A_2-to-B_3 molar ratio of 2:1, giving an anhydride-to-amino functional group ratio of 4:3, we obtained low polymerization yields (17 and 21%, respectively), with cross-linking polymerization occurring to provide PDs that could not be dispersed in water.

2.3. Particle Sizes and Zeta Potentials of PDs. DLS suggested that the particle sizes of PD-BT-12 and PD-ET-12 were both approximately 3 nm (Figure 3a,b). Moreover, TEM revealed that their particle sizes were approximately 3−5 nm (Figure 3c,d). Thus, our two types of polymers had hyperbranched structures and nanoscale dimensions of less than 10 nm, conforming to the definition of PDs.[30]

When synthesizing our PDs, we adopted an A_2-to-B_3 molar ratio of 1:2 to give an anhydride-to-amino functional group ratio of 1:3, resulting in peripheral amino groups on the nanoparticle surfaces. To examine the surface charges of the PDs, we dissolved PD-BT-12 and PD-ET-12 in water (1 mg mL^{-1}) and measured their zeta potentials, obtaining a value of −0.8 ± 0.2 mV for PD-BT-12 at pH 9.0 and a value of −2.9 ± 0.4 mV for PD-ET-12 at pH 8.4 (Figure S1a,b). We also examined the surface charges of the PDs in different aqueous environments. For solutions of PD-BT-12 at pH 4, 7, and 10, the measured zeta potentials were 42.2 ± 4.7, −1.1 ± 0.6, and −35.0 ± 2.5 mV, respectively; for PD-ET-12, the values were 46.7 ± 2.2, 2.6 ± 0.5, and −35.6 ± 3.8 mV, respectively. Thus,

https://doi.org/10.1021/acsomega.1c05537
ACS Omega 2021, 6, 33159−33170

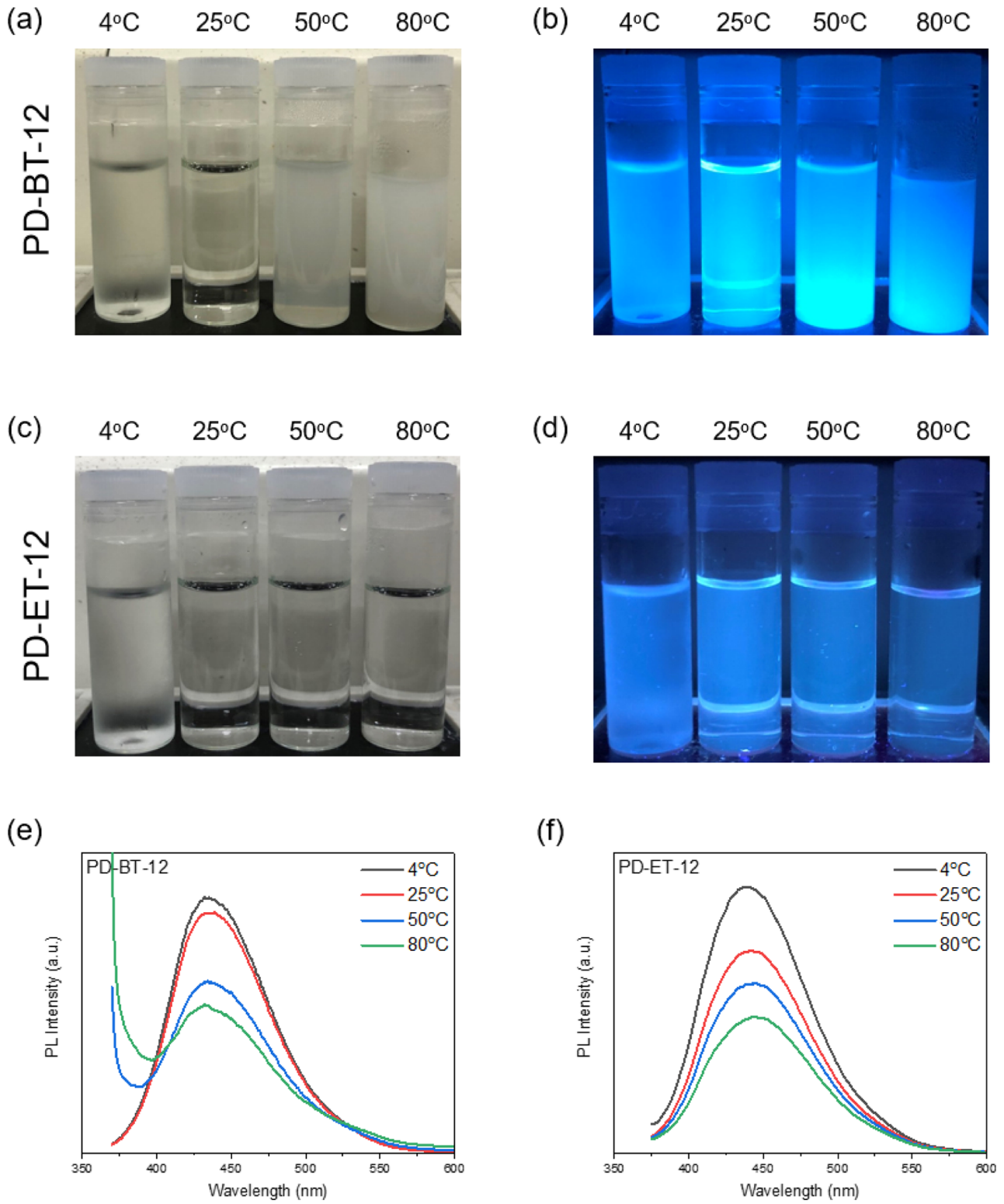

Figure 4. (a–d) Solutions of (a,b) PD-BT-12 and (c,d) PD-ET-12 that had been incubated at temperatures of 4, 25, 50, and 80 °C and photographed under (a,c) daylight and (b,d) UV light. (e,f) PL spectra of solutions of (e) PD-BT-12 and (f) PD-ET-12 recorded at temperatures of 4, 25, 50, and 80 °C.

the zeta potentials of the PD solutions increased upon decreasing the pH. This behavior is consistent with our PDs featuring both amino and carboxyl groups, which undergo protonation/deprotonation to give adjustable surface charges depending on the pH of the solution (Table S1).

2.4. Temperature and Concentration Effects on PDs.

Figure 4 reveals that solutions of our PDs (4 mg mL^{-1}) incubated at 4, 25, 50, and 80 °C displayed various appearances, from transparent to turbid, as a result of a solution interfacial phenomenon (cloud point behavior). The turbidity of the solution of PD-BT-12 increased significantly

https://doi.org/10.1021/acsomega.1c05537
ACS Omega 2021, 6, 33159−33170

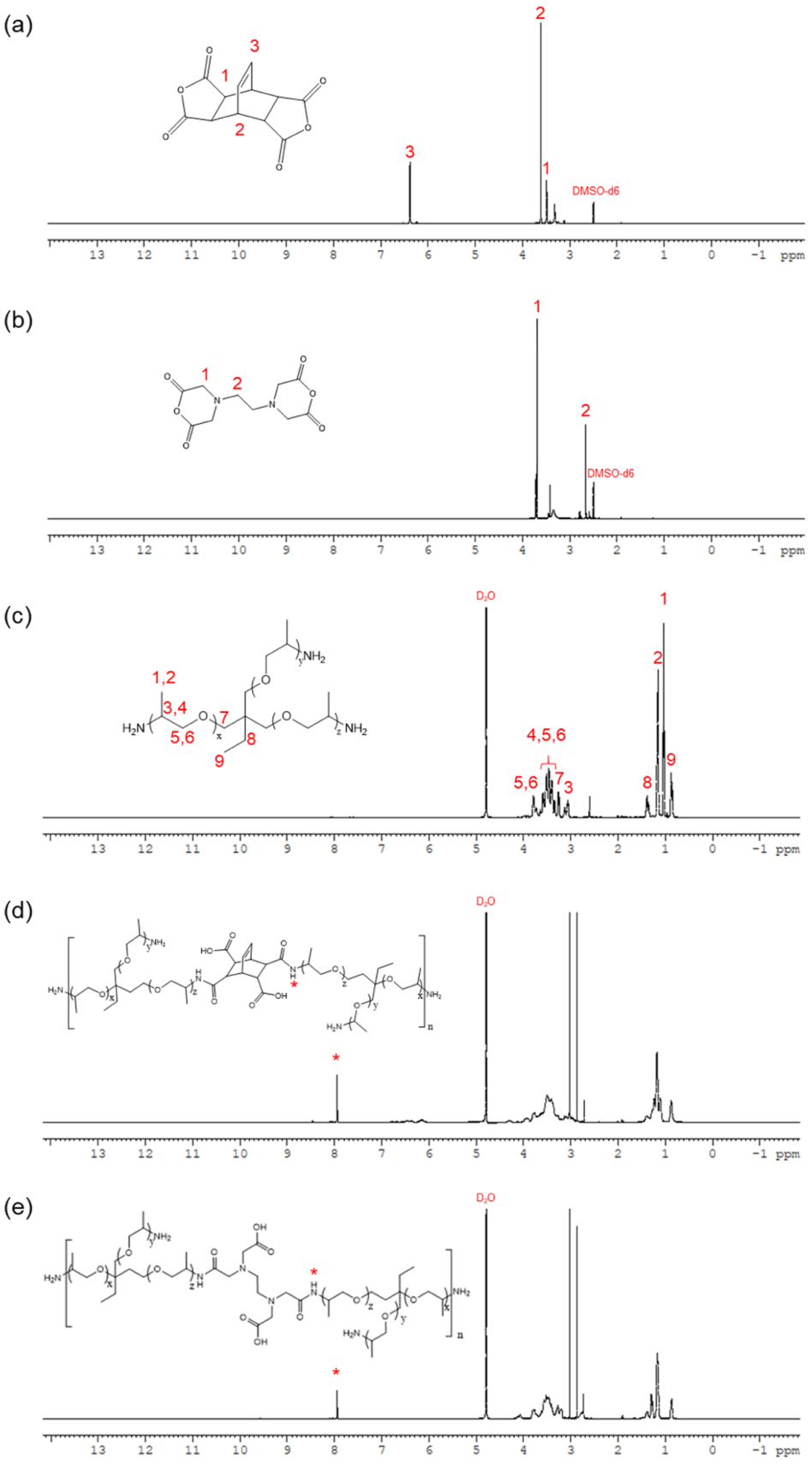

Figure 5. ^{1}H NMR spectra of (a) BCDA, (b) EDTAD, (c) Jeffamine T-403, (d) PD-BT-12, and (e) PD-ET-12.

from low to high temperature. Upon increasing the temperature, the intermolecular hydrogen bonds between the relatively rigid PD-BT-12 and the water molecules were broken, increasing the hydrophobicity of the PD and leading to

https://doi.org/10.1021/acsomega.1c05537
ACS Omega 2021, 6, 33159−33170

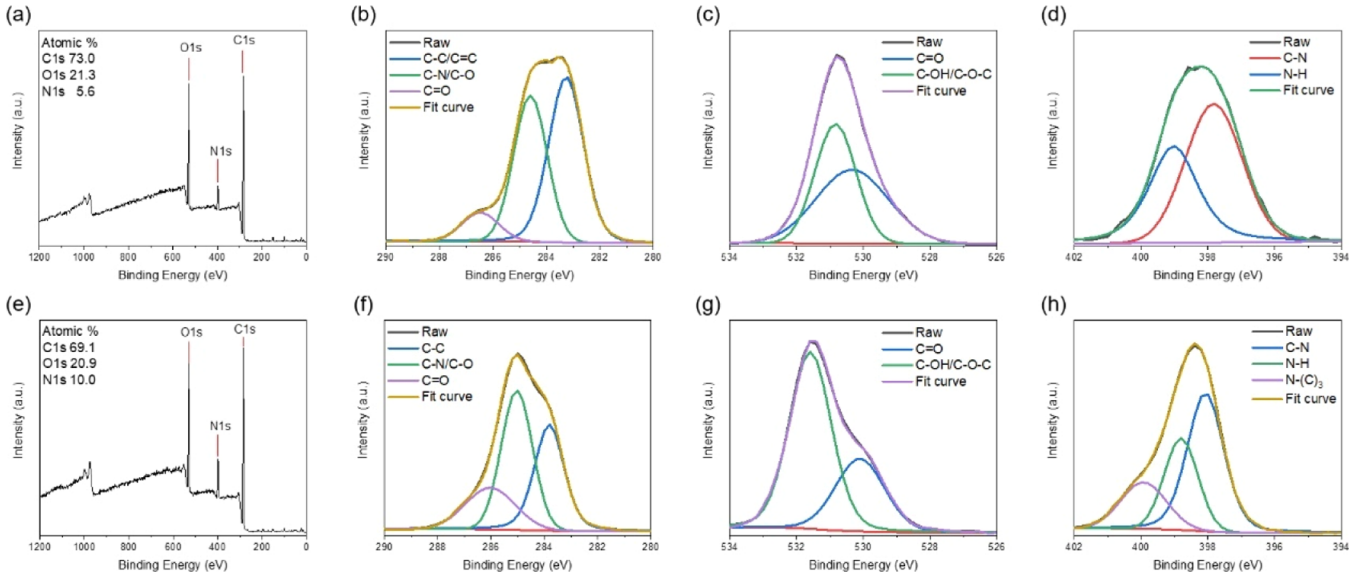

Figure 6. XPS spectra of (a−d) PD-BT-12 and (e−h) PD-ET-12: (a,e) survey spectra; (b,f) C 1s binding energies; (c,g) N 1s binding energies; and (d,h) O 1s binding energies.

lower fluorescence (Figure 4a,b).[31] In contrast, the transparency of the solution of PD-ET-12 was not affected by the temperature because the intermolecular hydrogen bonds between the PD and water molecules were more stable, which is the result of its relatively flexible molecular structure (Figure 4c,d). Nevertheless, the fluorescence intensities of PD-BT-12 and PD-ET-12 decreased upon proceeding from low to high temperature (Figure 4e,f). This phenomenon might have been due to disruption of the intramolecular hydrogen bonds between the carboxyl and amido groups of the PDs upon increasing the temperature of the solution, thereby minimizing the CTE effect and spatial conjugation behavior.[11,32−34] Moreover, the tendency for the decrease in the fluorescence intensity of PD-BT-12 from 4 to 25 °C was slower than that of PD-ET-12, presumably because of the former's relatively rigid molecular structure, but an obvious decrease in fluorescence intensity occurred from 25 to 50 °C because of the cloud point behavior.

Figure S2 displays the relationship between the fluorescence intensities of PD-BT-12 and PD-ET-12 and their concentrations from 0.05 to 4 mg mL^{-1}. The emission intensity increased upon increasing the concentrations of PD-BT-12 and PD-ET-12, revealing no quenching effects up to 4 mg mL^{-1}. Moreover, the fluorescence of the PDs was observable even when the concentration was 0.1 mg mL^{-1}.

2.5. Spectral Characterization of PDs. We recorded nuclear magnetic resonance (NMR), Fourier transform infrared (FTIR), and XPS spectra to confirm the structures of our PDs. A comparison of the ^{1}H NMR spectra of BCDA, EDTAD, Jeffamine T-403, and the PDs revealed that only those of the PDs featured signals at 7.94 ppm, representing the H atoms of their amido groups (Figure 5a−e).[35−38] Figure S3a displays the FTIR spectra of BCDA and EDTAD, featuring signals for the symmetric and asymmetric stretching of their C═O units in the ranges 1761−1774 and 1809−1822 cm^{-1}, respectively.[39,40] After the dianhydrides had reacted with the triamine to form poly(amic acid)s with amido and carboxyl groups, Figure S3b reveals that the FTIR spectra of PD-BT-12 and PD-ET-12 lacked any signals for symmetric and asymmetric stretching of the C═O units of the dianhydride but signals had emerged for amide I and II vibrational modes in the ranges 1543−1560 and 1657−1663 cm^{-1}, respectively.[41]

XPS revealed the functional groups and atomic compositions of the PD structures. The A_2 components of PD-ET-12 possessed tertiary amino groups, and the A_2 components of PD-BT-12 possessed bridged bicyclic alkene structures. Therefore, the different A_2 moieties led to different C 1s and N 1s compositions for these PDs. The XPS survey spectrum of PD-BT-12 revealed that its composition of C 1s (73.0%) was greater than that of PD-ET-12 (69.1%) and that the composition of N 1s of PD-ET-12 (10.0%) was greater than that of PD-BT-12 (5.6%) (Figure 6a,e). The C 1s spectrum of PD-BT-12 featured a signal for C−C/C═C bonds at 283.3 eV, consistent with the A_2 units of PD-BT-12 possessing C═C groups in a bridged bicyclic alkene structure; for PD-ET-12, a signal appeared for C−C bonds only (283.8 eV) (Figure 6b,f).[42−44] The O 1s spectra of PD-BT-12 and PD-ET-12 featured signals for C═O (530.3 and 530.1 eV) and C−OH/C−O−C (530.8 and 531.6 eV) bonds (Figure 6c,g).[45] The N 1s spectra of PD-BT-12 and PD-ET-12 featured signals for C−N (397.8 and 398.1 eV) and N−H (399.0 and 398.8 eV) bonds (Figure 6d,h).[46] Furthermore, the N 1s spectrum of PD-ET-12 featured a signal for N−$(C)_3$ bonds (399.9 eV), arising from the tertiary amino groups of its A_2 units (Figure 6h).[47] Thus, these NMR, FTIR, and XPS spectral analyses confirmed the syntheses of the two types of PDs, while TEM had confirmed the dispersion of their nanosized particles in aqueous solutions. Moreover, from the molecular structures and fluorescence properties of our PDs, we speculate that the clustering of C═O groups and branched N atoms within the nanoparticles—with their π-electrons and lone-pair (n) electrons experiencing spatial conjugation with restricted molecular motions and rotations in their nanoenvironments—resulted in their non-conventional fluorescence.[10,48]

2.6. Critical Micelle Concentrations of PDs. A PD that can undergo molecular self-assembly in aqueous solution will display a critical micelle concentration (CMC).[49,50] Surface tension measurements revealed that the CMCs of PD-BT-12 and PD-ET-12 were 0.07 and 0.12 mg mL^{-1}, respectively (Figure S4a,b). At 2 mg mL^{-1}, the surface tension of PD-BT-

https://doi.org/10.1021/acsomega.1c05537
ACS Omega 2021, 6, 33159−33170

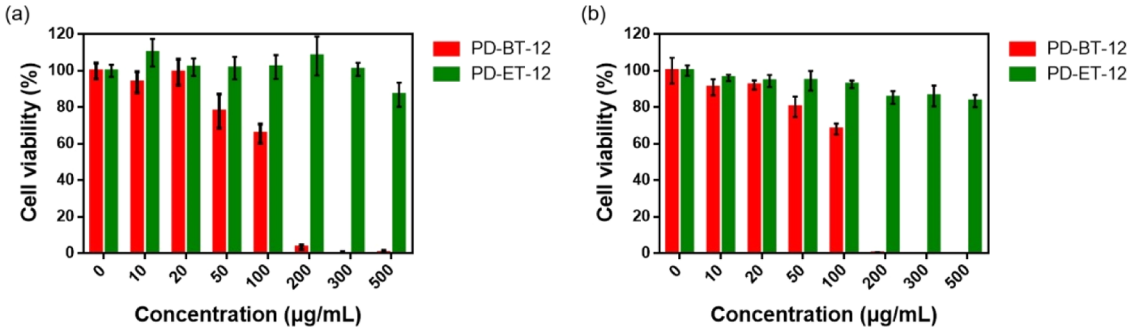

Figure 7. Viabilities of (a) MCF-7 and (b) HaCaT cells treated with PD-BT-12 and PD-ET-12 at various concentrations for 48 h.

12 (42 mN m^{-1}) was lower than that of PD-ET-12 (47 mN m^{-1}), due to their different interior chemical structures and physical properties.

2.7. Cytotoxicity of PDs. We used MTT assays to evaluate the cytotoxicity concentrations of our PDs toward a cancer cell line (MCF-7) and a normal cell line (HaCaT). Treating the MCF-7 and HaCaT cells with PD-BT-12 at 50 μg mL^{-1} for 48 h revealed that the cytotoxicity of PD-BT-12 was low; the cell viabilities were close to 80% at this concentration. The cell viabilities decreased to 70%, however, when the concentration of PD-BT-12 reached 100 μg mL^{-1}. PD-ET-12 displayed low cytotoxicity even when its concentration reached 500 μg mL^{-1} (Figure 7a,b). We suspect that the different molecular structures of PD-BT-12 and PD-ET-12—relatively rigid bridged bicyclic alkene and relatively flexible alkane structures, respectively—were responsible for these slight differences in cytotoxicity.

2.8. Bioimaging of PDs. To observe the labeling behavior of the PDs toward the cell lines, we treated the MCF-7 and HaCaT cells with PD-BT-12 and PD-ET-12 for 6 h. Because our MTT assays had demonstrated the cytotoxicity of PD-BT-12 at concentrations greater than 50 μg mL^{-1}, we treated the cells with our PDs at a concentration of 20 μg mL^{-1} in the incubation medium. We recorded confocal microscopy bioimages with excitation at 405 nm and emission at 420–480 nm. The confocal images in Figure 8a,b reveal clearly observed blue emissions upon excitation at 405 nm. When the bright field and fluorescence images were merged, the confocal images revealed that the fluorescence of PD-BT-12 and PD-ET-12 originated within the cells (Figure 8a,b). Thus, the MCF-7 and HaCaT cells could uptake PD-BT-12 and PD-ET-12, as determined through bioimaging, suggesting that both PDs might be potential fluorescent carriers for tracking and labeling. Moreover, the ability to adjust the net charges of these PDs suggests that they might function as carriers for various drugs, or as nanodrugs. Non-conventional PDs that display stable fluorescence without photobleaching have been suitable for use as long-term fluorescent nanocarriers.[34]

3. CONCLUSIONS

We have used an $A_2 + B_3$ strategy for the one-pot syntheses of two types of non-conventional fluorescent PDs possessing terminal amino functional groups, from commercially available dianhydrides (one with a bridged cyclic alkene and the other with a non-alkene) and the commercially available triamine T403. Although our PDs did not contain any π-conjugated systems, they displayed fluorescence, presumably because of their interior molecular clusters of C=O groups and branched N atoms, with the π-electrons and lone-pair (n) electrons experiencing a spatial conjugation with restricted molecular motion and rotation in their nanoenvironments, resulting in non-conventional fluorescence through a CTE effect. The fluorescence intensity of PD-ET-12 was affected by the pH of its environment; it dispersed well in water at various temperatures because of its relatively flexible structure. The physical behavior of PD-BT-12 was much different because of its relatively rigid bridged cyclic alkene structure. PD-BT-12 exhibited cytotoxicity at concentrations greater than 50 μg mL^{-1}, whereas PD-ET-12 displayed low cytotoxicity even at 500 μg mL^{-1}. Confocal microscopic bioimaging revealed that these PDs could be located within HaCaT and MCF-7 cells after a period of incubation. Although PD-BT-12 possessed relatively high cytotoxicity, it might be suitable as a nanodrug alone for selected cell lines or for conjugation with drugs or antibodies to target cancer sites or promote anticancer capability. PD-ET-12 might function as a low-cytotoxicity nanocarrier while also being suitable for conjugation with drugs and applied for bioimaging.

4. EXPERIMENTAL SECTION

4.1. Materials. Bicyclo[2.2.2]oct-7-ene-2,3,5,6-tetracarboxylic dianhydride (BCDA; molecular weight: 248.1 g mol^{-1}) was purchased from Alfa Aesar (Heysham, UK). Ethylenediaminetetraacetic dianhydride (EDTAD; molecular weight: 256.2 g mol^{-1}) was obtained from Tokyo Chemical Industry (Tokyo, Japan). Jeffamine T-403 (average molecular weight: 440 g mol^{-1}) was acquired from Huntsman (TX, USA). DMF was purchased from Duksan Pure Chemicals (South Korea). THF was obtained from Avantor Performance Materials (PA, USA). Dimethyl sulfoxide (DMSO) was acquired from Honeywell International (NJ, USA). DMSO-d_6 and deuterium oxide (D_2O) were purchased from Sigma-Aldrich (USA, MO). 3-(4,5-Dimethylthiazol-2-yl)-2,5-diphenyltetrazolium bromide (MTT) was obtained from Bio Basic (Markham, ON, Canada). Dulbecco's modified Eagle's medium (DMEM), fetal bovine serum (FBS), and antibiotic–antimycotic were acquired from Thermo Fisher Scientific (MA, USA). Phosphate-buffered saline (PBS) was purchased from Scientific Biotech (Taipei, Taiwan).

4.2. Synthesis of PDs. BCDA (0.50 g, 2.0 mmol) was dissolved in DMF (100 mL) under N_2, and Jeffamine T-403 (1.8 g, 4.0 mmol) was dissolved in THF (100 mL) under N_2. The solution of BCDA was added dropwise to the solution of Jeffamine T-403 at 0 °C. The mixture was warmed to room temperature with a total reaction time of 20 h. Separately, EDTAD (0.50 g, 2.0 mmol) was dissolved in DMF under N_2, and Jeffamine T-403 (1.8 g, 4.0 mmol) was dissolved in THF under N_2. The solution of EDTAD was added dropwise to the

https://doi.org/10.1021/acsomega.1c05537
ACS Omega 2021, 6, 33159−33170

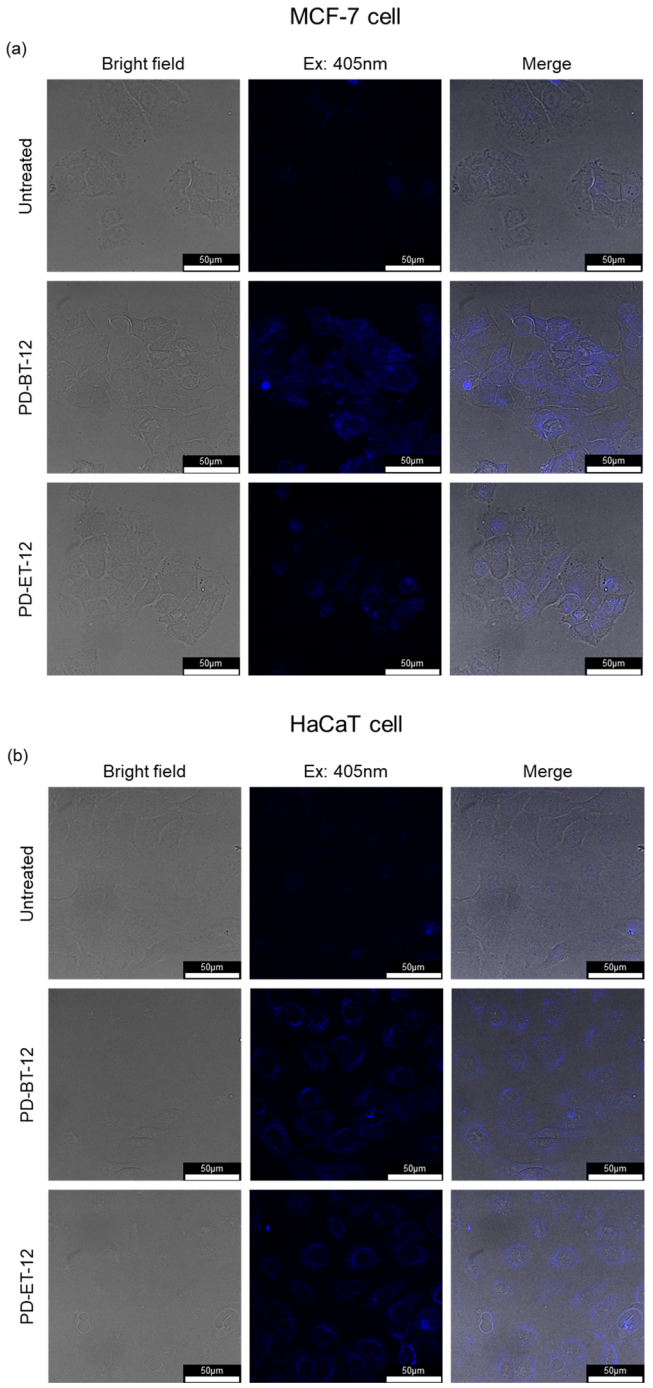

Figure 8. Confocal microscopy images of (a) MCF-7 and (b) HaCaT cells, untreated and treated with PD-BT-12 and PD-ET-12 for 6 h.

solution of Jeffamine T-403 at 0 °C in an ice bath, and then the temperature was increased slowly to room temperature, with a total reaction time of 20 h. In each case, the precipitates were filtered off and dissolved in water, and the solutions were subjected to dialysis through a membrane (molecular weight cut-off: 3500 g mol^{-1}) to remove any small molecules. The PD solutions were concentrated and then dried in a vacuum oven. The products are named herein as PD-BT-12 and PD-ET-12, respectively.

4.3. Characterization of PDs. The fluorescence and UV−vis spectra of the PDs were recorded using an F-2700 fluorescence spectrophotometer and a Lambda 265 UV−vis spectrophotometer (PerkinElmer), respectively. The particle sizes of the PDs were measured using a dynamic light scattering (DLS) instrument (Zetasizer Nano ZS90, Malvern). Transmission electron microscopy (TEM) was performed using a JEM-1400 microscope (Japan) operated at an acceleration voltage of 120 kV. Zeta potentials were recorded using a nanoPartica SZ-100V2 instrument (HORIBA). The structures of the PDs were identified using ^{1}H NMR spectroscopy (Agilent Technologies, 600 MHz), FTIR spectroscopy (IRAffinity-1S, Shimadzu), and XPS (PHI 5000 VersaProbe, ULVAC-PHI). Surface tensions were measured using a DST-30 digital surface tension analyzer (Surface Electro Optics). Confocal microscopy images were recorded using a Leica TCS SP8 X confocal spectral microscope imaging system and a white-light laser.

The QYs of the PDs were determined from the integrated fluorescence intensity and the absorption, according to the relative fluorescence QY equation

$$\phi_{PD} = \phi_{st}\cdot(I_{PD}/I_{st})\cdot(\eta/\eta_{st})^2$$

where Φ_{PD} is the QY of the PD, Φ_{st} is the QY of quinine sulfate in 0.1 M H_2SO_4 (Φ_{st} = 0.54), I is the slope of the plot of the integrated fluorescence intensity with respect to the absorbance, and η is the refractive index of the solvent.

4.4. Cytotoxicity of PDs (MTT Assay). The cytotoxicities of PD-BT-12 and PD-ET-12 toward MCF-7 and HaCaT cells were evaluated using an MTT assay. MCF-7 and HaCaT cells were seeded (5000 cells $well^{-1}$) in 96-well plates and cultured in fresh DMEM containing 10% FBS and 1% antibiotic at 37 °C under 5.0% CO_2 for 24 h. The concentrations of PD-BT-12 and PD-ET-12 in PBS were 20 and 25 mg mL^{-1}, respectively. The PD solutions were filtered through a 0.22 μm membrane. The MCF-7 and HaCaT cells were treated with PD-BT-12 and PD-ET-12 solutions of various concentrations (0, 10, 20, 50, 100, 200, 300, and 500 μg mL^{-1}) for 48 h. The MTT stock solution (5 mg mL^{-1}, 20 μL) was added to each well and reacted for 3 h. The supernatant was discarded and DMSO (200 μL) was added. A SpectraMax M2e spectrometer was used for the detection of the 96-well plates at OD_{570}.

4.5. Cell Imaging. PD-BT-12 and PD-ET-12 stock solutions (20 mg mL^{-1}) in PBS were filtered through a 0.22 μm membrane. MCF-7 and HaCaT cells were seeded (5×10^5 cells $well^{-1}$) in a six-well plate and cultured in fresh DMEM containing 10% FBS and 1% antibiotic at 37 °C under 5.0% CO_2 for 24 h. The MCF-7 and HaCaT cells were treated with the stock solutions of PD-BT-12 and PD-ET-12 for 6 h; the concentration of the PD in the medium was 20 μg mL^{-1}.

■ ASSOCIATED CONTENT

Supporting Information

The Supporting Information is available free of charge at https://pubs.acs.org/doi/10.1021/acsomega.1c05537.

PDs' zeta potentials in water at two different pH values, fluorescence spectra in aqueous solutions at various concentrations, FTIR spectra, surface tensions, and zeta potentials in aqueous solutions of various pH values (PDF)

https://doi.org/10.1021/acsomega.1c05537
ACS Omega 2021, 6, 33159−33170

AUTHOR INFORMATION

Corresponding Author

Tzong-Yuan Juang − *Department of Cosmeceutics, China Medical University, Taichung 40402, Taiwan;* orcid.org/0000-0001-6373-9687; Email: tyjuang@mail.cmu.edu.tw

Authors

Yu-Yu Chen − *Department of Cosmeceutics, China Medical University, Taichung 40402, Taiwan*

Siao-Cian Fan − *Department of Cosmeceutics, China Medical University, Taichung 40402, Taiwan*

Chang-Cheng Chang − *Aesthetic Medical Center, China Medical University Hospital, Taichung 40402, Taiwan; School of Medicine, China Medical University, Taichung 40402, Taiwan*

Jian-Cheng Wang − *Department of Cosmeceutics, China Medical University, Taichung 40402, Taiwan*

Hsiu-Mei Chiang − *Department of Cosmeceutics, China Medical University, Taichung 40402, Taiwan*

Complete contact information is available at: https://pubs.acs.org/10.1021/acsomega.1c05537

Notes

The authors declare no competing financial interest.

ACKNOWLEDGMENTS

This study was supported by research grants from the National Science Council of Taiwan (grant nos. MOST 108-2113-M-039-003 and MOST 110-2113-M-039-007) and China Medical University (grant nos. CMU108-AWARD-01 and CMU110-MF-124).

REFERENCES

(1) Fasbender, S.; Zimmermann, L.; Cadeddu, R.-P.; Luysberg, M.; Moll, B.; Janiak, C.; Heinzel, T.; Haas, R. The Low Toxicity of Graphene Quantum Dots is Reflected by Marginal Gene Expression Changes of Primary Human Hematopoietic Stem Cells. *Sci. Rep.* **2019**, *9*, 12028.

(2) Li, Y.-J.; Harroun, S. G.; Su, Y.-C.; Huang, C.-F.; Unnikrishnan, B.; Lin, H.-J.; Lin, C.-H.; Huang, C.-C. Synthesis of Self-Assembled Spermidine-Carbon Quantum Dots Effective against Multidrug-Resistant Bacteria. *Adv. Healthcare Mater.* **2016**, *5*, 2545−2554.

(3) Lo, P.-Y.; Lee, G.-Y.; Zheng, J.-H.; Huang, J.-H.; Cho, E.-C.; Lee, K.-C. GFP Plasmid and Chemoreagent Conjugated with Graphene Quantum Dots as a Novel Gene Delivery Platform for Colon Cancer Inhibition In Vitro and In Vivo. *ACS Appl. Bio Mater.* **2020**, *3*, 5948−5956.

(4) Liu, Y.; Huang, H.; Cao, W.; Mao, B.; Liu, Y.; Kang, Z. Advances in carbon dots: from the perspective of traditional quantum dots. *Mater. Chem. Front.* **2020**, *4*, 1586−1613.

(5) Chen, Y.-Y.; Jiang, W.-P.; Chen, H.-L.; Huang, H.-C.; Huang, G.-J.; Chiang, H.-M.; Chang, C.-C.; Huang, C.-L.; Juang, T.-Y. Cytotoxicity and cell imaging of six types of carbon nanodots prepared through carbonization and hydrothermal processing of natural plant materials. *RSC Adv.* **2021**, *11*, 16661−16674.

(6) Liu, Z.; Li, B.; Shi, X.; Li, L.; Feng, Y.; Jia, D.; Zhou, Y. Target-oriented synthesis of high synthetic yield carbon dots with tailored surface functional groups for bioimaging of zebrafish, flocculation of heavy metal ions and ethanol detection. *Appl. Surf. Sci.* **2021**, *538*, 148118.

(7) Zan, M.; An, S.; Cao, L.; Liu, Y.; Li, L.; Ge, M.; Liu, P.; Wu, Z.; Dong, W.-F.; Mei, Q. One-pot facile synthesis of yellow-green emission carbon dots for rapid and efficient determination of progesterone. *Appl. Surf. Sci.* **2021**, *566*, 150686.

(8) Sharma, V.; Tiwari, P.; Mobin, S. M. Sustainable carbon-dots: recent advances in green carbon dots for sensing and bioimaging. *J. Mater. Chem. B* **2017**, *5*, 8904−8924.

(9) Bauri, K.; Saha, B.; Banerjee, A.; De, P. Recent advances in the development and applications of nonconventional luminescent polymers. *Polym. Chem.* **2020**, *11*, 7293−7315.

(10) Du, Y.; Yan, H.; Huang, W.; Chai, F.; Niu, S. Unanticipated strong blue photoluminescence from fully biobased aliphatic hyperbranched polyesters. *ACS Sustainable Chem. Eng.* **2017**, *5*, 6139−6147.

(11) Ye, R.; Liu, Y.; Zhang, H.; Su, H.; Zhang, Y.; Xu, L.; Hu, R.; Kwok, R. T. K.; Wong, K. S.; Lam, J. W. Y.; Goddard, W. A.; Tang, B. Z. Non-conventional fluorescent biogenic and synthetic polymers without aromatic rings. *Polym. Chem.* **2017**, *8*, 1722−1727.

(12) Zhu, S.; Song, Y.; Shao, J.; Zhao, X.; Yang, B. Non-Conjugated Polymer Dots with Crosslink-Enhanced Emission in the Absence of Fluorophore Units. *Angew. Chem., Int. Ed.* **2015**, *54*, 14626−14637.

(13) Shiau, S.-F.; Juang, T.-Y.; Chou, H.-W.; Liang, M. Synthesis and properties of new water-soluble aliphatic hyperbranched poly(amido acids) with high pH-dependent photoluminescence. *Polymer* **2013**, *54*, 623−630.

(14) Liu, T.; Meng, Y.; Wang, X.; Wang, H.; Li, X. Unusual strong fluorescence of a hyperbranched phosphate: discovery and explanations. *RSC Adv.* **2013**, *3*, 8269−8275.

(15) Jiang, N.; Zhu, D.; Su, Z.; Bryce, M. R. Recent advances in oligomers/polymers with unconventional chromophores. *Mater. Chem. Front.* **2021**, *5*, 60−75.

(16) Chen, X.; Yang, T.; Lei, J.; Liu, X.; Zhao, Z.; Xue, Z.; Li, W.; Zhang, Y.; Yuan, W. Z. Clustering-Triggered Emission and Luminescence Regulation by Molecular Arrangement of Nonaromatic Polyamide-6. *J. Phys. Chem. B* **2020**, *124*, 8928−8936.

(17) Zhang, H.; Zhao, Z.; Turley, A. T.; Wang, L.; McGonigal, P. R.; Tu, Y.; Li, Y.; Wang, Z.; Kwok, R. T. K.; Lam, J. W. Y.; Tang, B. Z. Aggregate Science: From Structures to Properties. *Adv. Mater.* **2020**, *32*, 2001457.

(18) Miao, X.; Liu, T.; Zhang, C.; Geng, X.; Meng, Y.; Li, X. Fluorescent aliphatic hyperbranched polyether: chromophore-free and without any N and P atoms. *Phys. Chem. Chem. Phys.* **2016**, *18*, 4295−4299.

(19) Sun, B.; Zhao, B.; Wang, D.; Wang, Y.; Tang, Q.; Zhu, S.; Yang, B.; Sun, H. Fluorescent non-conjugated polymer dots for targeted cell imaging. *Nanoscale* **2016**, *8*, 9837−9841.

(20) Juang, T.-Y.; Hsu, Y.-C.; Jiang, B.-H.; Chen, C.-P. Highly Efficient Inverted Organic Photovoltaics Containing Aliphatic Hyperbranched Polymers as Cathode Modified Layers. *Macromolecules* **2016**, *49*, 7837−7843.

(21) Wang, R.-b.; Yuan, W.-z.; Zhu, X.-y. Aggregation-induced emission of non-conjugated poly (amido amine) s: discovering, luminescent mechanism understanding and bioapplication. *Chin. J. Polym. Sci.* **2015**, *33*, 680−687.

(22) Pastor-Pérez, L.; Chen, Y.; Shen, Z.; Lahoz, A.; Stiriba, S.-E. Unprecedented Blue Intrinsic Photoluminescence from Hyperbranched and Linear Polyethylenimines: Polymer Architectures and pH-Effects. *Macromol. Rapid Commun.* **2007**, *28*, 1404−1409.

(23) Zhao, E.; Lam, J. W. Y.; Meng, L.; Hong, Y.; Deng, H.; Bai, G.; Huang, X.; Hao, J.; Tang, B. Z. Poly [(maleic anhydride)-alt-(vinyl acetate)]: A pure oxygenic nonconjugated macromolecule with strong light emission and solvatochromic effect. *Macromolecules* **2015**, *48*, 64−71.

(24) Zheng, Y.; Li, S.; Weng, Z.; Gao, C. Hyperbranched polymers: advances from synthesis to applications. *Chem. Soc. Rev.* **2015**, *44*, 4091−4130.

(25) Unal, S.; Oguz, C.; Yilgor, E.; Gallivan, M.; Long, T. E.; Yilgor, I. Understanding the structure development in hyperbranched polymers prepared by oligomeric A2+ B3 approach: comparison of experimental results and simulations. *Polymer* **2005**, *46*, 4533−4543.

(26) Saraiva, M. A. Interpretation of α-synuclein UV absorption spectra in the peptide bond and the aromatic regions. *J. Photochem. Photobiol., B* **2020**, *212*, 112022.

(27) Chen, F.; Jiang, H.; Chen, W.; Huang, G. Interaction of the synthetic antithrombotic peptide P10 with thrombin: a spectroscopy study. *RSC Adv.* **2019**, *9*, 18498−18505.
(28) Liao, J.; Cheng, Z.; Zhou, L. Nitrogen-Doping Enhanced Fluorescent Carbon Dots: Green Synthesis and Their Applications for Bioimaging and Label-Free Detection of Au3+ Ions. *ACS Sustainable Chem. Eng.* **2016**, *4*, 3053−3061.
(29) Wang, D.; Imae, T. Fluorescence emission from dendrimers and its pH dependence. *J. Am. Chem. Soc.* **2004**, *126*, 13204−13205.
(30) Zhu, S.; Song, Y.; Zhao, X.; Shao, J.; Zhang, J.; Yang, B. The photoluminescence mechanism in carbon dots (graphene quantum dots, carbon nanodots, and polymer dots): current state and future perspective. *Nano Res.* **2015**, *8*, 355−381.
(31) Duester, L.; Fabricius, A.-L.; Jakobtorweihen, S.; Philippe, A.; Weigl, F.; Wimmer, A.; Schuster, M.; Nazar, M. F. Can cloud point-based enrichment, preservation, and detection methods help to bridge gaps in aquatic nanometrology? *Anal. Bioanal. Chem.* **2016**, *408*, 7551−7557.
(32) Chen, X.; Liu, X.; Lei, J.; Xu, L.; Zhao, Z.; Kausar, F.; Xie, X.; Zhu, X.; Zhang, Y.; Yuan, W. Z. Synthesis, clustering-triggered emission, explosive detection and cell imaging of nonaromatic polyurethanes. *Mol. Syst. Des. Eng.* **2018**, *3*, 364−375.
(33) Vallan, L.; Urriolabeitia, E. P.; Ruipérez, F.; Matxain, J. M.; Canton-Vitoria, R.; Tagmatarchis, N.; Benito, A. M.; Maser, W. K. Supramolecular-enhanced charge transfer within entangled polyamide chains as the origin of the universal blue fluorescence of polymer carbon dots. *J. Am. Chem. Soc.* **2018**, *140*, 12862−12869.
(34) Chatterjee, D. P.; Pakhira, M.; Nandi, A. K. Fluorescence in "Nonfluorescent" Polymers. *ACS Omega* **2020**, *5*, 30747−30766.
(35) Capezza, A. J.; Cui, Y.; Numata, K.; Lundman, M.; Newson, W. R.; Olsson, R. T.; Johansson, E.; Hedenqvist, M. S. High Capacity Functionalized Protein Superabsorbents from an Agricultural Co-Product: A Cradle-to-Cradle Approach. *Adv. Sustainable Syst.* **2020**, *4*, 2000110.
(36) Tang, S.; Shi, Z.; Cao, Y.; He, W. Facile aqueous-phase synthesis of multi-responsive nanogels based on polyetheramines and bisepoxide. *J. Mater. Chem. B* **2013**, *1*, 1628−1634.
(37) Padavan, D. T.; Wan, W. K. Synthesis and characterization of a novel versatile poly (amic acid) derived from ethylenediaminetetra-acetic dianhydride. *Mater. Chem. Phys.* **2010**, *124*, 427−433.
(38) Faghihi, K.; Shabanian, M. Preparation of new optically active and thermally stable poly (amide-imide) containing bicyclo segment and ether group in the main chain by direct polycondensation in two different media. *J. Chil. Chem. Soc.* **2010**, *55*, 491−496.
(39) Yan, J.; Zhang, B.; Wang, Z. Monodispersed ultramicroporous semi-cycloaliphatic polyimides for the highly efficient adsorption of CO_2, H_2 and organic vapors. *Polym. Chem.* **2016**, *7*, 7295−7303.
(40) Tiptipakorn, S.; Punuch, W.; Okhawilai, M.; Rimdusit, S. Property enhancement of polybenzoxazine modified with monoanhydrides and dianhydrides. *J. Polym. Res.* **2015**, *22*, 1−11.
(41) Tang, Y.; Zhou, X.; Xu, K.; Dong, X. One-pot synthesis of fluorescent non-conjugated polymer dots for Fe3+ detection and temperature sensing. *Spectrochim. Acta, Part A* **2020**, *240*, 118626.
(42) Tammina, S. K.; Yang, D.; Li, X.; Koppala, S.; Yang, Y. High photoluminescent nitrogen and zinc doped carbon dots for sensing Fe3+ ions and temperature. *Spectrochim. Acta, Part A* **2019**, *222*, 117141.
(43) Boruah, A.; Saikia, M.; Das, T.; Goswamee, R. L.; Saikia, B. K. Blue-emitting fluorescent carbon quantum dots from waste biomass sources and their application in fluoride ion detection in water. *J. Photochem. Photobiol., B* **2020**, *209*, 111940.
(44) Hong, G.-L.; Zhao, H.-L.; Deng, H.-H.; Yang, H.-J.; Peng, H.-P.; Liu, Y.-H.; Chen, W. Fabrication of ultra-small monolayer graphene quantum dots by pyrolysis of trisodium citrate for fluorescent cell imaging. *Int. J. Nanomed.* **2018**, *13*, 4807.
(45) Yu, J.; Song, N.; Zhang, Y.-K.; Zhong, S.-X.; Wang, A.-J.; Chen, J. Green preparation of carbon dots by Jinhua bergamot for sensitive and selective fluorescent detection of Hg2+ and Fe3+. *Sens. Actuators, B* **2015**, *214*, 29−35.
(46) Gao, Z.; Zhao, C.-x.; Li, Y.-y.; Yang, Y.-l. Beer yeast-derived fluorescent carbon dots for photoinduced bactericidal functions and multicolor imaging of bacteria. *Appl. Microbiol. Biotechnol.* **2019**, *103*, 4585−4593.
(47) Zhao, X.; Li, J.; Liu, D.; Yang, M.; Wang, W.; Zhu, S.; Yang, B. Self-Enhanced Carbonized Polymer Dots for Selective Visualization of Lysosomes and Real-Time Apoptosis Monitoring. *iScience* **2020**, *23*, 100982.
(48) Lu, H.; Feng, L.; Li, S.; Zhang, J.; Lu, H.; Feng, S. Unexpected strong blue photoluminescence produced from the aggregation of unconventional chromophores in novel siloxane−poly (amidoamine) dendrimers. *Macromolecules* **2015**, *48*, 476−482.
(49) Jin, X.; Sun, P.; Tong, G.; Zhu, X. Star polymer-based unimolecular micelles and their application in bio-imaging and diagnosis. *Biomaterials* **2018**, *178*, 738−750.
(50) Qi, M.; Zhou, Y. Multimicelle aggregate mechanism for spherical multimolecular micelles: from theories, characteristics and properties to applications. *Mater. Chem. Front.* **2019**, *3*, 1994−2009.

https://doi.org/10.1021/acsomega.1c05537
ACS Omega 2021, 6, 33159−33170